A novel ClpC adaptor protein that functions in the developing *Bacillus subtilis* spore

Shawn C. Massoni[1,*], Nicola Evans[2,*], Ingo Hantke[3], Colleen Fenton[1], James H. Torpey[2], Katherine M. Collins[2], Ewelina M. Krysztofinska[2], Janina H. Muench[2], Arjun Thapaliya[2], Santiago Martínez-Lumbreras[2], Sé Hart Martin[1], Christopher B. Prior[4], Kürşad Turgay[3,5], Rivka L. Isaacson[2], and Amy H. Camp[1,#]

[1]Department of Biological Sciences, Mount Holyoke College, South Hadley MA
[2]Department of Chemistry, Faculty of Natural, Mathematical and Engineering Sciences, King's College London, London, UK
[3]Institute for Microbiology, Leibniz Universität Hannover, Hannover, Germany
[4]Department of Mathematical Sciences, Durham University, Durham, UK
[5]Max Planck Unit for the Science of Pathogens, Berlin, Germany
*These authors contributed equally to this work

[#]Address correspondence to Amy H. Camp (acamp@mtholyoke.edu) or Rivka L. Isaacson (rivka.isaacson@kcl.ac.uk)

Running title: YjbA is a sporulation-specific ClpC adaptor protein

Keywords: *Bacillus subtilis*, sporulation, protein degradation, AAA+ protease, adaptor protein, ClpC, YjbA

ABSTRACT

Bacterial protein degradation machinery, which comprises mix-and-match chaperone-protease pairs, plays vital roles in the bacterial life-cycle, and its manipulation has begun to spark interest as an alternative antimicrobial strategy. ClpC-ClpP (ClpCP) is one such chaperone-protease, recruited by adaptors to specific functions in the Gram positive model bacterium *Bacillus subtilis*. Using genetic approaches, we have identified a new adaptor protein, YjbA, that recruits ClpCP during sporulation, a developmental process by which *B. subtilis* can wait out unfavorable environmental conditions by becoming hardy, dormant spores. A knockout of *yjbA* strongly stimulates gene expression in the developing spore; conversely, aberrant overexpression of *yjbA* during vegetative growth is toxic. A combination of *in vivo* and *in vitro* experiments demonstrates that YjbA and ClpC directly interact, and that this interaction induces ClpC oligomerization and ATPase activity. Finally, a co-crystal structure reveals that YjbA binds to the ClpC N-terminal domain at a location distinct from that bound by the well-characterized adaptor protein MecA, but similar to the interaction site on the *Mycobacterium tuberculosis* ClpC1 N-terminal domain where bactericidal cyclic peptides bind. Based on these data, we speculate that YjbA induces ClpCP to degrade substrate proteins in the developing spore, thereby facilitating steps towards metabolic dormancy.

INTRODUCTION

Cells across all domains of life employ AAA+ proteases to degrade misfolded or aggregated proteins, as well as to control the abundance of specific proteins and, in turn, the myriad biological processes they regulate (Sauer and Baker 2011; Yedidi et al. 2017; Zhang and Mao 2020). The most complex and perhaps best-known AAA+ protease, the 26S proteasome, is responsible for the majority of protein degradation in eukaryotic cells, regulating essential processes including the cell cycle, signal transduction, and apoptosis (Bard et al. 2018; Collins and Goldberg 2017). In bacteria, the degradation of key proteins by a more diverse set of AAA+ proteases (e.g. Clp, Lon, FtsH proteases) drives cell division, biofilm formation, pathogenesis, competence, and other developmental processes (Mahmoud and Chien 2018). Given their far-reaching roles in cell physiology, AAA+ proteases are attractive therapeutic targets. For example, proteasome inhibitors have been used with success to treat certain human cancers (Fricker 2020; Goldberg 2012), and natural products that dysregulate bacterial AAA+ proteases can act as antibiotics against pathogens such as *Mycobacterium tuberculosis* and *Staphylococcus aureus* (Culp and Wright 2017; Raju et al. 2012).

Like the proteasome, bacterial AAA+ proteases are large barrel-like molecular machines with both chaperone and protease domains (reviewed in (Mahmoud and Chien 2018)). The Hsp100 chaperone, a member of the AAA+ (ATPases associated with various cellular activities) superfamily, forms a hexamer and uses conformational changes induced by the binding and hydrolysis of ATP to unfold and translocate protein substrates through its central pore and into the interior chamber of the protease, where the proteolytic active sites are buried. Unlike eukaryotic proteins, which are marked for proteasomal degradation by the covalent attachment of ubiquitin, bacterial proteins are typically recognized for degradation by their cognate AAA+

protease through intrinsic peptide sequences (“degrons”) to which the chaperone component binds directly or indirectly via one or more adaptor proteins (Kuhlmann and Chien 2017).

In Gram positive bacteria including the model bacterium *Bacillus subtilis* and pathogens *Staphylococcus aureus* and *Listeria monocytogenes*, the ClpC-ClpP (ClpCP) protease, composed of the AAA+ chaperone ClpC and the protease ClpP, plays a central role in both general and regulatory proteolysis, in turn impacting numerous cellular pathways including stress resistance, competence, sporulation, and virulence (Biørnstad and Håvarstein 2011; Birk et al. 2021; Gunaratnam et al. 2019; Krüger et al. 1994; Mashruwala et al. 2019; Msadek et al. 1994; Rouquette et al. 1998). In *M. tuberculosis*, the equivalent protease (ClpC1P1P2) is essential and is the target of bactericidal cyclic peptides cyclomarin A, ecumicin, lassomycin, and rufomycin (Choules et al. 2019; Gao et al. 2015; Gavrish et al. 2014; Schmitt et al. 2011).

The ClpC chaperone protein harbors two AAA+ ATPase domains, termed D1 and D2, that form stacked rings in the active hexamer (Sauer and Baker 2011; Wang et al. 2011). Loops within D2 allow the ClpC hexamer to dock onto two stacked heptameric rings of the ClpP protease. ClpC additionally contains a coiled-coil M domain (also referred to as the “linker”) embedded within D1, as well as an N-terminal domain (“N-domain”) that sits atop the D1 ring and mediates selection of substrates for degradation. In some cases, the N-domain directly interacts with substrates, for example those that are marked with a phosphorylated arginine (pArg) residue (Trentini et al. 2016). In other cases, the ClpC N-domain indirectly interacts with substrates via adaptor proteins such as MecA, which recruits the *B. subtilis* competence master regulator ComK and other substrates for ClpCP-mediated degradation (Turgay et al. 1998).

Here we report the characterization of a novel ClpCP adaptor protein, YjbA, that we identified in a genetic screen for factors that help drive metabolic differentiation during *B. subtilis* endospore formation. The process of sporulation, which is triggered by starvation, involves a

well-characterized sequence of morphological events (Fig 1A) (Tan and Ramamurthi 2014; Riley et al. 2020). First, asymmetric division gives rise to a small cell (the forespore) that develops into the mature, metabolically-dormant, and environmentally-resistant spore, and a larger cell (the mother cell) that aids in the development of the spore but ultimately dies. Next, the mother cell engulfs the forespore giving rise to a cell-within-a-cell configuration. Finally, the forespore acquires protective peptidoglycan cortex and protein coat layers, and is released into the environment upon lysis of the mother cell.

These morphological events of sporulation are driven by hundreds of genes expressed under the control by four alternative sigma (σ) factors that are sequentially activated in the forespore (σ^F at early times, followed by σ^G at later times) and mother cell (σ^E at early times, followed by σ^K at later times (Arrieta-Ortiz et al. 2015; de Hoon et al. 2010). Interestingly, σ^G-dependent gene expression at late times in the forespore relies upon the transport of small molecule building blocks from the mother cell via an intercellular channel comprised of the mother cell proteins SpoIIIAA-AH and the forespore protein SpoIIQ (Camp and Losick 2009; Morlot and Rodrigues 2018; Riley et al. 2021; Zeytuni and Strynadka 2020).

The ClpCP protease, among other AAA+ proteases, has been previously implicated in *B. subtilis* sporulation. Mutants lacking *clpC* or *clpP* display sporulation defects, the *clpC* gene is transcribed at early times in the forespore under σ^F-dependent control, and the ClpCP protease is preferentially active in the forespore relative to the mother cell (Arrieta-Ortiz et al. 2015; Kain et al. 2008; Meeske et al. 2016; Msadek et al. 1998; Wang et al. 2006).

Here we provide evidence that the previously uncharacterized protein YjbA, which is expressed under σ^F-dependent control at early times in the forespore, functions as a novel adaptor for the *B. subtilis* ClpCP protease. YjbA facilitates oligomerization and ATPase activity of ClpC, similarly to the well-characterized ClpC adaptor MecA. Yet a co-crystal structure

reveals that YjbA binds to the ClpC N-terminal domain at a site distinct from that bound by MecA, but analogous to the site at which the bactericidal cyclic peptides target the *M. tuberculosis* ClpC1 (Wolf et al. 2020, 2019; Vasudevan et al. 2013; Wang et al. 2011). Given the *in vivo* sporulation phenotypes of *B. subtilis* cells lacking *yjbA*, we speculate that YjbA induces ClpCP to degrade substrate proteins in the developing spore, the removal of which dampens its capacity to carry out gene expression and, perhaps, sets it on the path to metabolic dormancy.

MATERIALS AND METHODS

General *B. subtilis* methods

Information regarding strains, plasmids, primers, and synthetic DNA fragments used in this study are provided in Supplemental Materials. To measure competence, cells were transformed as previously described (Wilson and Bott 1968) with 500 ng of plasmid pDG1730 (*amyE*::*spc*) (Guérout-Fleury et al. 1996); transformation efficiency was calculated as the number of transformants divided by the total number of viable cells. To quantify spore formation, cells were induced to sporulate by nutrient exhaustion for 24 h at 37°C in Difco sporulation medium (DSM) (Nicholson and Setlow 1990; Schaeffer et al. 1965), after which the number of colony forming units (CFU)/mL that survived heat treatment (80°C for 20 min) was determined. For other experiments, including β-galactosidase activity assays and fluorescence microscopy, sporulation was induced by the resuspension method (Nicholson and Setlow 1990; Sterlini and Mandelstam 1969). Cells were collected at intervals by centrifugation and either processed immediately or stored at -80°C for later analysis. β-galactosidase activity in samples from *B. subtilis* strains harboring *lacZ* reporters was measured as previously described (Camp and Losick 2009). Details regarding microscopy are provided in Supplemental Materials and Methods.

Bacterial two-hybrid assay

Bacterial two-hybrid assays (Dove and Hochschild 2004) were carried out in the *Escherichia coli* strain FW102 O_L2-62 (Deaconescu et al. 2006) as detailed in Supplemental Materials and Methods. The full list of bacterial two hybrid plasmids and resulting bacterial two hybrid strains are provided in Supplemental Tables S2 and Supplemental Table S6, respectively.

Isothermal Titration Calorimetry (ITC)

YjbA, $ClpC^{N}$, or $ClpC^{N,Q11P}$ were purified as described in Supplemental Materials and Methods (final buffer conditions: 50 mM Tris pH 8.85, 150 mM NaCl, 50 mM L-Glu, 0.5 mM TCEP). ITC experiments were performed at 25°C using an ITC-200 MicroCal microcalorimeter (GE Healthcare) following a standard procedure (Hands-Taylor et al. 2010). In each titration, 20 injections of YjbA at a concentration of 700 μM were added to ClpC constructs at 70 μM in the reaction cell. Integrated heat data obtained for the titrations, corrected for heats of dilution, were fitted using a nonlinear least-squares minimization algorithm to a theoretical titration curve, using the MicroCal-Origin 7.0 software package.

Analytical Size Exclusion Chromatography (SEC)

Analytical SEC experiments with YjbA, MecA, and $ClpC^{DWB}$ (purified as described in Supplemental Materials and Methods) were performed on a Superose 6 10/300 Increase column (GE Healthcare) at 4°C. Proteins were diluted to 10 μM in column running buffer (50 mM Tris pH 8.0, 300 mM NaCl, 5 mM $MgCl_2$, 0.5 mM DTT, 0.5 mM ATP) and incubated 10 min with 5 mM ATP at 37°C as previously described (Kirstein et al. 2006). 1 mL fractions were collected and the proteins were precipitated using trichloroacetic acid (final 10%) and acetone, and analyzed by SDS-PAGE and Coomassie staining. Additional SEC methods are provided in Supplemental Materials and Methods.

ATPase and Protein Degradation Assays

In vitro ATPase assays were performed as previously described (Lanzetta et al. 1979; Turgay et al. 1997). ClpC, $ClpC^{Q11P}$, or $ClpC^{Q11A}$ proteins (1 μM each; purified as described in

Supplemental Materials and Methods) were mixed with MecA (1 μM) or YjbA (1-15 μM) in ATPase assay buffer (50 mM Tris pH 8.0, 50 mM KCl, 5 mM $MgCl_2$). Reactions were started by addition of ATP to a final concentration of 4 mM, at 37°C. Reactions were stopped by adding 10 μL of the reaction mixture to 160 μL staining solution (3.4 mg/L malachite green, 10.5 g/L ammonium molybdate, and 0.1% Triton X-100 in 1 N HCl) in a 96-well plate, followed by the addition of 20 μL 34% (w/v) sodium citrate. Released phosphate was measured by absorbance at 660 nm. ATPase activity was calculated from the linear slope between the 0 min and 5 min time points of the reaction.

Protein Degradation Assays

Degradation assays were performed in ATPase assay buffer (50 mM Tris pH 8.0, 50 mM KCl, 5 mM $MgCl_2$) with an ATP regeneration system (Schlothauer et al. 2003) and all proteins (purified as described in Supplemental Materials and Methods) diluted to 1 μM. Reactions were started at 37°C by adding ATP to a final concentration of 4 mM. Samples were taken at indicated time points for analysis by SDS-PAGE followed by Coomassie staining.

Protein Crystallography

The YjbA/$ClpC^N$ complex crystallized at 8.4 mg/mL in 2.0 M $(NH_4)_2SO_4$, 100 mM NaOAc, pH 4.6. PDB: 5HBN (Trentini et al. 2016) was used as an initial molecular replacement model for $ClpC^N$. For further details on screening, data collection, processing and model-building, see Supplemental Materials and Methods.

RESULTS

Deletion of the *yjbA* gene significantly stimulates forespore gene expression.

At the outset of this study, we conducted a screen to identify genes involved in metabolic shutdown of the developing *B. subtilis* forespore. We hypothesized that such genes would be under the control of the early-acting forespore sigma factor σ^F given that the forespore soon thereafter becomes dependent upon its connection to the mother cell—via the SpoIIIAA-AH•SpoIIQ channel—for late gene expression (Fig 1A). We therefore tested deletion mutants of 59 known or predicted σ^F target genes for phenotypes indicating a possible role in metabolic shutdown. Details regarding the original genetic screen are provided in Supplemental Materials (Fig S1, Table S5).

Most notably, we found that deletion of the gene *yjbA* caused significantly stimulated forespore gene expression, a phenotype we speculated could be consistent with a role in metabolic shutdown. Cells deleted for *yjbA* displayed a ~10-fold increase in the σ^F-dependent expression of P_{spoIIQ}-*lacZ* (Fig 1B), and a small but reproducible ~1.6-fold increase in the σ^G-dependent expression of P_{sspB}-*lacZ* (Fig 1C); these effects were fully complemented by a wild-type copy of *yjbA*. Similar results were observed for other σ^F- and σ^G-dependent reporters (Fig S2A, S2B). In contrast, σ^E- and σ^K-dependent mother cell gene expression was mostly normal in Δ*yjbA* cells (Fig S2C, S2D).

The *yjbA* gene has until now remained uncharacterized other than its assignment to the σ^F regulon by transcriptomic studies (Arrieta-Ortiz et al. 2015; Steil et al. 2005; Wang et al. 2006). We found that *yjbA* upstream regulatory sequences, including a putative σ^F consensus promoter sequence (Fig S3A) (Sierro et al. 2008), ribosome binding site (RBS), and ATG start codon, drove expression of a *lacZ* reporter gene beginning at hour 2 of sporulation, consistent with the timing of σ^F activity (Fig S3B). Moreover, β-galactosidase production was blocked in

cells deleted for the gene encoding σ^F, but not those encoding σ^E, σ^G, or σ^K (Fig S3B). When these same upstream regulatory sequences were fused to a *gfp* reporter gene, GFP was detectable by fluorescence microscopy in the forespore at around the start of engulfment, consistent with both the location and timing of σ^F activity (Fig S3D).

The *B. subtilis yjbA* open reading frame encodes a protein of 250 amino acids with a predicted molecular weight of 30 kDa. NCBI BLAST analysis (Altschul et al. 1990) revealed that YjbA is well-conserved among members of the *Bacilliaceae* family (Fig S4), but that YjbA is not found encoded in the genomes of endospore-formers of the more distantly-related *Clostridia* genus. A search against the NCBI Conserved Domains Database (CDD) (Marchler-Bauer et al. 2017) yielded no findings other than the DUF3603 superfamily (Domain Accession pfam12227; *E*-value 3.09e-146), which comprises other YjbA homologs.

To monitor the YjbA protein during sporulation, we constructed a *gfp-yjbA* fusion gene expressed under the *yjbA* regulatory sequences described above and confirmed its functionality (Fig S3C). By fluorescence microscopy, GFP-YjbA was first detected in forespores during early engulfment and appeared to be enriched at the forespore membrane (Fig S3E). According to the PolyPhobius predictor program, YjbA does not harbor any signal peptides nor transmembrane regions (Käll et al. 2005), suggesting that YjbA may be a peripheral forespore membrane protein. We also noted that GFP-YjbA fluorescence was nearly an order of magnitude dimmer than the GFP reporter described above (Fig S3D vs. Fig S3E). Given that both GFP and GFP-YjbA were expressed from the same *yjbA* regulatory sequences, these findings suggest that the YjbA protein may be targeted for degradation in the forespore.

Finally, we found that Δ*yjbA* mutants were modestly deficient for spore formation, producing ~20-30% fewer heat-resistant spores than wild type cells in single-round sporulation assays (Fig S5A). The Δ*yjbA* mutant also displayed a competitive disadvantage relative to wild

type cells during multiple rounds of growth and sporulation in co-culture (Fig S5B, S5C). This indicates that *yjbA* contributes to maximal sporulation efficiency, consistent with the sporulation-specific expression of *yjbA*, its effect upon forespore gene expression, and its conservation in the spore-forming *Bacilliaceae* family.

Vegetative expression of *yjbA* causes cell filamentation and lysis by a mechanism requiring the ClpCP AAA+ protease.

We next constructed a strain in which *yjbA* could be expressed during vegetative growth under the control of an isopropyl-β-D-thiogalactoside [IPTG]-inducible promoter. When grown on solid media with high concentrations of IPTG (1 mM), this strain formed small colonies that lysed after 1-2 days at 37°C; at lower concentrations of IPTG (10-100 μM), growth appeared mostly normal (Fig 2A, Fig S6A). However, when observed by phase microscopy, cells from colonies grown at lower inducer concentrations were noticeably elongated, and individual lysed cells were also observed (Fig 2B, Fig S6B). Fluorescence microscopy revealed that the elongated cells were aseptate filaments that sometimes harbored evenly spaced nucleoids (Fig S6C). A GFP fusion to the FtsZ-associated protein ZapA displayed a diffuse localization in these cells, indicating a failure to form the FtsZ ring ("Z-ring") responsible for the initiation of cell division in nearly all bacteria (Fig S6C) (Gueiros-Filho and Losick 2002; Haeusser and Margolin 2016). We therefore conclude that expression of *yjbA* during vegetative growth interferes with Z-ring assembly, which likely accounts for the observed filamentous phenotype.

To identify the YjbA target(s) that drive cell filamentation and toxicity, we isolated extragenic suppressor mutations that restored normal growth to cells overexpressing *yjbA*. This genetic strategy was facilitated by the spontaneous appearance of such suppressors (Fig 2A, Fig S6A, inset), although we did modify our *yjbA* overproducing strain to minimize isolation of

intragenic mutations in the expression construct itself (see Supplemental Materials and Methods). We found that extragenic suppression of *yjbA* vegetative toxicity was most commonly caused by mutations in the *clpC* gene. ClpC is a member of the Hsp100 family of AAA+ chaperones that partners with the ClpP protease to degrade target proteins (reviewed in (Sauer and Baker 2011)). Notably, a strain deleted for *clpC* was protected against the colony lysis and cell filamentation phenotypes associated with *yjbA* expression (Fig 2B-C). Cells deleted for *clpP*, despite displaying a small colony phenotype even in the absence of inducer, were also immune to the toxic effects of *yjbA* expression (Fig 2B). These genetic data indicate that YjbA induces filamentation and toxicity in vegetative cells by a mechanism that requires the ClpCP proteolytic complex.

The *yjbA*-specific *clpC*^{Q11P} allele phenocopies Δ*yjbA* during sporulation.

Most of our isolated *clpC* suppressor alleles (5 out of 6) harbored mutations predicted to severely compromise ClpC function (e.g. truncations, insertions) (see Table S1 for more details). However, one isolated allele, *clpC*^{Q11P}, fully suppressed *yjbA*-associated toxicity and filamentation through a single point mutation in the codon for Gln11, switching it to proline (Q11P) (Fig 2A-B). Gln11 is located in the ClpC N-terminal domain ("N-domain") responsible for binding substrates and/or adaptor proteins that recruit substrates to the protease complex (Fig 2C) (Kojetin et al. 2009; Mogk et al. 2004; Trentini et al. 2016; Wang et al. 2011). Interestingly, *clpC*^{Q11P} did not cause pleiotropic defects associated with *clpC* loss-of-function such as reduced competence and sporulation efficiency (Fig 2D-E) (Meeske et al. 2016; Msadek et al. 1998; Nanamiya et al. 1998; Pan et al. 2001), suggesting that *clpC*^{Q11P} is likely to be a *yjbA*-specific *clpC* allele. Consistent with a specific interaction at Gln11, we found that its substitution for alanine (Q11A) also suppressed *yjbA*-associated toxicity (Fig 2A).

We reasoned that the *yjbA*-specific *clpC*^{Q11P} allele would allow us to assess whether YjbA mediates its effects on forespore physiology in collaboration with ClpCP, which is known to be present and active in the forespore during sporulation (Kain et al. 2008; Pan et al. 2001; Pan and Losick 2003), without the complication of other pleiotropic defects of a Δ*clpC* mutant. Strikingly, the *clpC*^{Q11P} allele caused the same stimulation of forespore gene expression as observed in Δ*yjbA* cells (Fig 2F). In contrast, the Δ*clpC* mutant did not exhibit any stimulation of σ^F activity, but rather a modest delay (Fig 2F), consistent with known pleiotropic sporulation defects of Δ*clpC* cells, including delayed entry and defects in engulfment and σ^G activation (Meeske et al. 2016; Msadek et al. 1998; Nanamiya et al. 1998; Pan et al. 2001), and further supports the notion that *clpC*^{Q11P} is a *yjbA*-specific *clpC* allele. Finally, no additional σ^F activity was observed in a Δ*yjbA clpC*^{Q11P} double mutant (Fig 2F), suggesting that *yjbA* and *clpC* likely operate in the same pathway to regulate forespore gene expression.

YjbA interacts with the ClpC N-domain in a Gln11-dependent manner

To determine whether YjbA directly interacts with the ClpC N-domain (ClpC^N), we purified recombinant versions of each protein and analyzed their association through several approaches. When YjbA and ClpC^N were combined at different molar ratios and subjected to analytical size exclusion chromatography (SEC), formation of a higher molecular weight YjbA-ClpC^N complex was evident (Fig S7). Next, we used nuclear magnetic resonance (NMR) to collect heteronuclear single quantum coherence (HSQC) spectra of ^{15}N-labeled ClpC^N or ^{15}N-labeled ClpC^{N,Q11P} (harboring the Q11P substitution) alone and in combination with increasing molar ratios of unlabeled YjbA (Fig S8). The addition of YjbA altered the ClpC^N spectrum, indicating complex formation; in contrast, the ClpC^{N,Q11P} spectrum remained stable in the presence of YjbA at four-fold molar excess, suggesting that the Q11P substitution disrupted

interaction (Fig S8C vs. Fig S8D). Finally, we employed isothermal titration calorimetry (ITC) to confirm a weak binding interaction between YjbA and $ClpC^{N}$ (K_d = 3.79 μM), while the $ClpC^{N,Q11P}$ variant was unable to interact (Fig 3A).

To further explore the interaction between ClpC and YjbA, we made use of a transcription activation-based bacterial (*E. coli*) two-hybrid assay (Dove and Hochschild 2004). When full-length ClpC and YjbA were paired as bait and prey, we observed a nearly 4-fold stimulation of reporter gene expression relative to a negative control strain (Fig 3B), consistent with an interaction. To identify the region(s) of ClpC required to interact with YjbA, we constructed ClpC bait variants harboring one or more of its multiple domains: the aforementioned adaptor/substrate-binding N-domain, the two AAA+ ATPase domains (D1 and D2), and a short linker domain (M) embedded within the D1-domain (Fig 2C and Fig 3B). We found that YjbA interacted with ClpC variants harboring the N-domain ($ClpC^{N}$ and $ClpC^{ND1M}$) but not those lacking the N-domain ($ClpC^{D1M}$ and $ClpC^{D2}$) (Fig 3B). The ClpC N-domain is therefore both necessary and sufficient for interaction with YjbA in this assay, consistent with our in vitro data. We noted, however, that YjbA interacted more robustly with $ClpC^{ND1M}$ relative to $ClpC^{N}$ (4-fold vs. 2-fold stimulation of reporter gene expression, respectively), suggesting that YjbA may also make stabilizing contacts with the ClpC D1- and/or M-domains (Fig 3B). Regardless, the interaction of YjbA with all ClpC variants harboring the N-domain was significantly reduced (full-length ClpC) or became undetectable ($ClpC^{ND1M}$ and $ClpC^{N}$) when the Q11P substitution was introduced (Fig 3B), indicating that ClpC Gln11 is required for (robust) interaction with YjbA.

Finally, we used the same bacterial 2-hybrid assay to compare the interaction of ClpC with YjbA to its well-characterized adaptor protein MecA (Schlothauer et al. 2003; Wang et al. 2011). Consistent with the known interaction between these two proteins, β-galactosidase production was stimulated nearly 5-fold relative to the negative control strain when ClpC and

MecA were paired as bait and prey (Fig 3B). Also as predicted from previous studies, MecA interacted with ClpC variants harboring the N- or D1M-domains ($ClpC^{N}$, $ClpC^{ND1M}$, $ClpC^{D1M}$), but did not interact with a ClpC variant harboring only the D2 domain ($ClpC^{D2}$) (Fig 3B) (Kirstein et al. 2006; Wang et al. 2011). In contrast to YjbA, the interactions of MecA with full-length ClpC, $ClpC^{ND1M}$, and $ClpC^{N}$ were either unaffected ($ClpC^{ND1M}$ and $ClpC^{N}$) or even slightly stimulated (full-length ClpC) by the Q11P substitution (Fig 3B). These data reveal that the ClpC interaction with YjbA is distinct from its interaction with MecA, most notably in that the ClpC N-domain residue Gln11 is specifically required for interaction with YjbA.

YjbA induces oligomerization and ATPase activity of full-length ClpC *in vitro*.

The genetic and physical interaction between YjbA and ClpC suggested to us a working model in which YjbA binds to and modulates the activity of the ClpCP proteolytic complex in the forespore. In one version of this model, YjbA could function as a novel adaptor protein, binding to the ClpC N-domain and recruiting one or more substrates for degradation by ClpCP. To test this idea, we first implemented size exclusion chromatography to determine whether YjbA could induce the formation of higher oligomeric complexes of ClpC *in vitro*. We used a ClpC E280A/E618A double walker B variant ($ClpC^{DWB}$), which binds but does not hydrolyze ATP and is known to form more stable higher oligomeric complexes with its adaptor protein MecA (Kirstein et al. 2006). Strikingly, $ClpC^{DWB}$ formed large oligomeric complexes when mixed with YjbA in equimolar concentrations in the presence of ATP (Fig 4A-B) (Kirstein et al. 2006).

A second hallmark of ClpC adaptor proteins, including MecA, is their ability to induce ClpC ATPase activity (Schlothauer et al. 2003). We found that YjbA induced the ATPase activity of ClpC, albeit to a lesser extent than MecA (Fig 4C). Increasing the relative concentration of YjbA led to a maximum ClpC ATPase rate that was approximately one third of that induced by

MecA. ClpC^{Q11P} ATPase activity could not be induced by either MecA or YjbA, suggesting that this mutant is nonfunctional under these *in vitro* conditions. However, a ClpC^{Q11A} variant was induced by MecA but not by YjbA. (Note that the *clpC^{Q11A}* mutant is indistinguishable from the *clpC^{Q11P}* mutant in suppressing *yjbA*-induced toxicity during vegetative growth [Fig 2A].)

Finally, given that YjbA forms a higher oligomeric complex with ClpC and induces its ATPase activity, we wondered whether ClpC in complex with its cognate protease, ClpP, would degrade YjbA and/or a test substrate *in vitro*. Unlike MecA, however, YjbA was not degraded by ClpCP nor did it act as an adaptor for α/β-casein degradation (Fig 4D-E) (Schlothauer et al. 2003).

Co-crystal structure of ClpC^{N} and YjbA

Finally, we solved the X-ray crystal structure of YjbA in complex with ClpC^{N}, a 1:1 heterodimer, at 2.0 Å resolution (deposited as PDB: 8B3S; Fig 5A). ClpC^{N} overlays with an RMSD of 1.56 Å to a previously reported ClpC^{N} structure (PDB: 2Y1Q) (Wang et al. 2011). YjbA consists of an N-terminal domain (YjbA^{N}, residues 1-135) and a C-terminal domain (YjbA^{C}, residues 143-250), connected by a disordered linker. YjbA^{N} includes a small antiparallel beta-barrel and an isolated beta hairpin surrounded by three alpha-helices, while YjbA^{C} is an alpha-helical bundle. Both YjbA domains make contacts with ClpC^{N}, fixing their positions relative to one another. The structure of YjbA is novel, with no significant structural homologs found for the full-length protein when queried against PDBeFold, Dali, and BioXGEM 3D-BLAST servers (Holm and Laakso 2016; Krissinel and Henrick 2004; Tung et al. 2007; Yang and Tung 2006). When the YjbA domains were analyzed individually, the N-domain still returned no significant structural homologs, whereas the C-domain exhibited structural similarity to a variety of

helical-bundle-containing proteins including members of the eukaryotic death domain (DD) superfamily, such as RIP, CARD and Pyrin type proteins (Park et al. 2016).

The interface between YjbA and $ClpC^N$ covers 1360 $Å^2$, and involves a combination of hydrophobic and electrostatic interactions (Fig 5B-D), the latter including three basic side chains on ClpC (K12, H79, and K85) that are within hydrogen bonding distance of three corresponding acidic side chains on YjbA (E161, E53, and E116). Interestingly, ClpC Gln11 does not bind directly to YjbA but rather does so indirectly via a network of water molecules (Fig 5E); as noted above, the adjacent residue K12 appears to directly interact with YjbA (Fig 5D). When queried, AlphaFold Multimer (Evans et al. 2022) was unable to predict the same binding interface, and instead positions $ClpC^N$ with low confidence on the opposite surface of YjbA. The $ClpC^N$ binding surface occupied by YjbA in our co-crystal structure is distinct from that bound by other known $ClpC^N$ protein interactors (MecA and phosphoarginine-modified proteins) (Wang et al. 2011; Trentini et al. 2016), but is analogous to the surface of *M. tuberculosis* ClpC1 that is bound by various antibiotics (cyclomarin A, ecumicin, rufomycin) (Vasudevan et al. 2013; Wolf et al. 2020, 2019) (Fig 6).

To examine the effect of the $clpC^{Q11P}$ mutation, we also solved the crystal structure of $ClpC^{N,Q11P}$ to 1.2 Å resolution (deposited as PDB: 8OTK). It closely resembles previous ClpC structures with the exception of a slight kink in the first alpha-helix at the location of the Q11P substitution (Fig S9).

Despite extensive efforts we were unable to crystallize YjbA in isolation, which we believe is a consequence of the mobility conferred on YjbA by the flexible linker that connects its two domains. AlphaFold (Jumper et al. 2021) predicts the YjbA monomer as being essentially structurally identical to how it appears in the complex crystal structure (overlaying with RMSD = 1.0), including the orientation of the two domains relative to one another. However, when we

performed small-angle X-ray scattering (SAXS) on YjbA, the results were incompatible with the rigid AlphaFold and complex crystal structures (Fig S10), supporting the idea that the N- and C-domains of YjbA can move around via the linker in the absence of a binding partner.

DISCUSSION

Although AAA+ protease systems are known to be important for successful sporulation in *B. subtilis*, limited information exists on the pathways and adaptors that implement their actions. Here, we have identified and characterized a novel ClpC adaptor protein, YjbA, that functions in the developing *B. subtilis* spore, but causes toxicity when ectopically expressed in vegetative cells. Genetic approaches revealed the connection between the AAA+ chaperone ClpC and YjbA and we subsequently showed that YjbA binds directly to ClpC, inducing its oligomerization and ATPase activity. This interaction can be specifically abolished with a single amino acid substitution at Gln11 in ClpC. Finally, we solved a co-crystal structure of YjbA bound to the ClpC N-domain, revealing that YjbA binds to a surface of the ClpC N-domain that is unique among its known adaptor proteins but that overlaps with the homologous binding sites of three antibiotics known to misregulate the *M. tuberculosis* ClpC1 protein (Fig 6) (Trentini et al. 2016; Vasudevan et al. 2013; Wang et al. 2011; Wolf et al. 2020, 2019).

How does YjbA bind and activate ClpC?

Our study adds YjbA to a growing list of proteins and small molecules that bind to and activate ClpC. Structural and other studies have revealed that these binding partners can induce ClpC to adopt a variety of assembly states. On its own, ClpC can form an inactive resting decamer state (Carroni et al. 2017; Morreale et al. 2022). Binding partners that activate ClpC drive it out of the resting state to an active hexamer or even tetramer of hexamers (Morreale et al. 2022; Maurer et al. 2019; Carroni et al. 2017). The best studied ClpC-binding protein is the MecA adaptor, which activates *B. subtilis* ClpC by driving its assembly into a functional hexamer, with MecA binding in a 1:1 ratio with ClpC N-domains and M-domain linkers (Carroni et al. 2017; Kirstein et al. 2006; Wang et al. 2011). Substrate proteins that have been phosphorylated by

McsB on arginine residues can also drive ClpC to assemble into an active hexamer (Trentini et al. 2016).

YjbA triggers ClpC hexamerization and ATPase activity, analogous to the classical *B. subtilis* ClpC adaptor MecA (Wang et al. 2011). However, our solved $ClpC^{N}$-YjbA structure is sterically incompatible with published structures of the ClpC hexamer formed through binding with MecA. As shown in Figure 7, when we dock YjbA onto the ClpC hexamer using the ClpC N-domain for alignment, we observe clashes between YjbA and the ClpC M-domain. However, the ClpC N-domain is separated from the rest of the protein by a 15-residue flexible linker, which likely allows its repositioning (Wang et al. 2011). The M-domain has also been demonstrated to move by 6.0 Å during substrate processing, which might also accommodate YjbA binding (Liu et al. 2013). It is interesting to consider the possibility that, like MecA, YjbA may interact with the M-domain, which could explain our bacterial two-hybrid data that YjbA binds better to $ClpC^{ND1M}$ than to $ClpC^{N}$ alone. This would also suggest a mechanism by which YjbA promotes hexamerization and activation of ClpC, given that assembly of the inactive ClpC state requires head-to-head M-domain interactions (Carroni et al. 2017). Future determination of the full YjbA-ClpC assembled structure, likely using cryo-electron microscopy to observe multiple states, will prove informative both in observing the structural differences as compared to other adaptors but also in understanding the mechanism of YjbA-induced ClpC activation.

The significance of YjbA binding to a surface of $ClpC^{N}$ that overlaps with the homologous binding sites of three antibiotics that target *M. tuberculosis* ClpC1 is unclear. Even among these antibiotics, binding at this surface results in different effects upon ClpC1 and the ClpC1-ClpP1-ClpP2 (ClpC1P1P2) proteolytic complex. The cyclic peptide cyclomarin A increases both the ATPase of ClpC1 and proteolytic activity of ClpC1P1P2, such that substrate specificity is relaxed (Maurer et al. 2019; Taylor et al. 2022); in contrast, the cyclic peptides

ecumicin and rufomycin decrease ClpC1P1P2 proteolytic activity, while either increasing (ecumicin) or leaving unaffected (rufomycin) ClpC1 ATPase activity (Gao et al. 2015; Choules et al. 2019). Like cyclomarin A and ecumicin, we have found that YjbA stimulates ClpC ATPase activity, but have so far been unable to demonstrate the ability of YjbA to stimulate ClpCP proteolysis. We nevertheless infer that YjbA exerts its *in vivo* effects by promoting (as opposed to inhibiting) ClpCP-mediated proteolysis, given our genetic finding that deletion of either *clpC* or *clpP* suppresses vegetative toxicity of *yjbA* overexpression. It is tempting to speculate that YjbA, like cyclomarin A, might constitutively activate ClpCP-dependent proteolysis, but we find this unlikely given that YjbA could not stimulate ClpCP to degrade casein *in vitro*.

What is the *in vivo* role of YjbA-ClpCP during sporulation?

Several lines of evidence support a critical role for AAA+ protease-mediated protein turnover during *B. subtilis* sporulation. First, mutants lacking *clpP*, *clpX*, *clpC*, and *ftsH* display severely reduced sporulation efficiency (Deuerling et al. 1997; Gerth et al. 1998; Le and Schumann 2009; Liu et al. 1999; Meeske et al. 2016; Msadek et al. 1998; Tan et al. 2015). Second, *clpC* and *lonB*, are expressed under the control of the early-acting forespore alternative sigma (σ) factor σ^F (Arrieta-Ortiz et al. 2015; Kain et al. 2008; Serrano et al. 2001; Steil et al. 2005; Wang et al. 2006). Finally, several sporulation-specific AAA+ protease substrates have been identified, including Sda (degraded by ClpXP at the onset of sporulation (Ruvolo et al. 2006)), SpoIIE (degraded by FtsH in the mother cell after asymmetric division (Bradshaw and Losick 2015)), SpoIIAB (degraded by ClpCP in the forespore after asymmetric division (Pan et al. 2001)), and SpoIVA (degraded, if misassembled, by ClpXP in the mother cell after engulfment (Tan et al. 2015)). Other proteins—including σ^F, σ^E, and multiple metabolic

enzymes—have been shown to disappear during sporulation, with the protease responsible yet to be identified (Fujita and Losick 2002; Ju et al. 1998; Magnin et al. 1997; Riley et al. 2021).

We propose that YjbA is a sporulation-specific adaptor protein for ClpCP, recruiting and triggering the degradation of proteins in the developing spore. Which proteins might be targeted for degradation by YjbA-adapted ClpCP? We have shown here that in Δ*yjbA* or *clpC*^{Q11P} mutant cells, forespore gene expression is significantly stimulated at both early (σ^F-dependent) and late (σ^G-dependent) times. This phenotype suggests that YjbA-ClpCP ordinarily dampens forespore gene expression, for example by degrading one or more proteins that positively regulate transcription and/or translation. One candidate target protein could be σ^F itself. Indeed, σ^F levels decrease in the forespore, suggesting proteolysis (Magnin et al. 1997). We further speculate that YjbA-ClpCP may also be degrading general metabolic enzymes that have recently been shown to disappear from the forespore at exactly the time YjbA-ClpCP would be active (Riley et al. 2021). Degradation of these types of proteins could explain the vegetative toxicity caused by overexpression of *yjbA* and may provide a compelling working model for how metabolic shutdown is driven during sporulation.

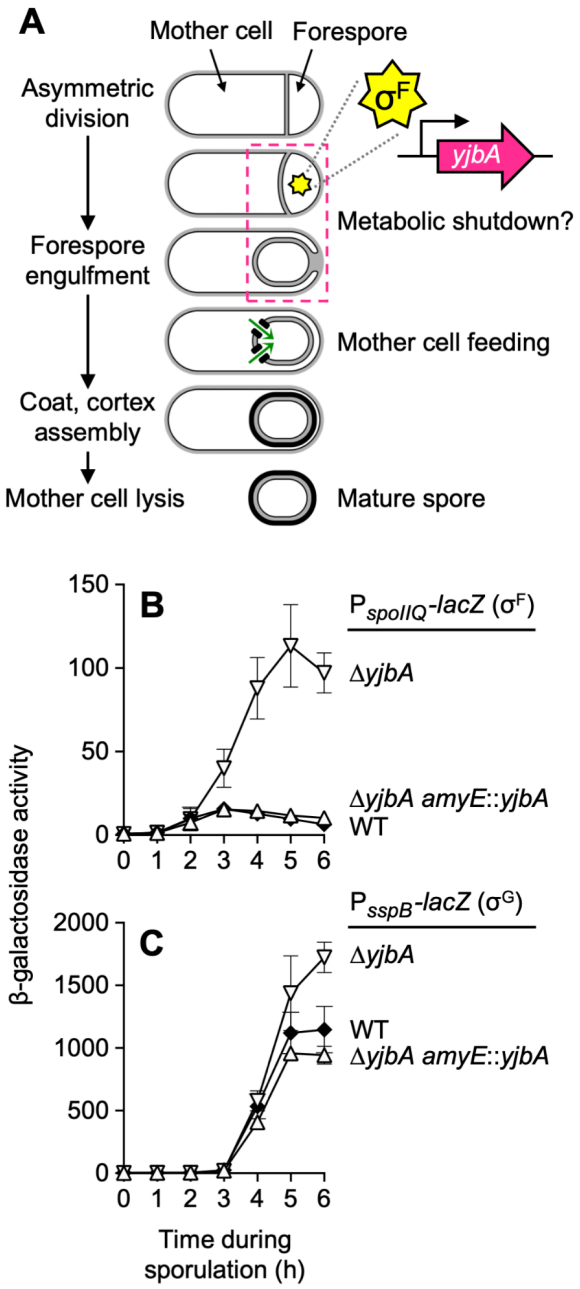

Figure 1. Forespore gene expression is stimulated in cells deleted for *yjbA*.
(A) Cartoon representation of *B. subtilis* sporulation, with major morphological events indicated. Also shown is the channel apparatus through which the mother cell is thought to sustain the forespore during its final stages of development (Camp and Losick 2009; Riley et al. 2021). The early-acting forespore sigma factor σ^F is shown, as is the *yjbA* gene, which has been assigned to the σ^F regulon (Arrieta-Ortiz et al. 2015; Steil et al. 2005; Wang et al. 2006) and is the focus of this study.

(B,C) The forespore-specific sigma factors σ^F and σ^G are significantly more active in Δ*yjbA* cells. Production of β-galactosidase from the **(B)** σ^F-dependent P_{spoIIQ}-*lacZ* reporter or **(C)** σ^G-dependent P_{sspB}-*lacZ* reporter was monitored during sporulation of otherwise wild type cells (WT; closed diamonds), cells deleted for *yjbA* (Δ*yjbA*; open inverted triangles), or cells deleted for *yjbA* and harboring *yjbA* integrated at the *amyE* locus (Δ*yjbA amyE*::*yjbA*; open triangles) (P_{spoIIQ}-*lacZ* strains AHB1841, CFB530, and CFB541, respectively; P_{sspB}-*lacZ* strains AHB324, SMB179, and SMB334, respectively). Error bars indicate ± standard deviations based on three or more independent experiments.

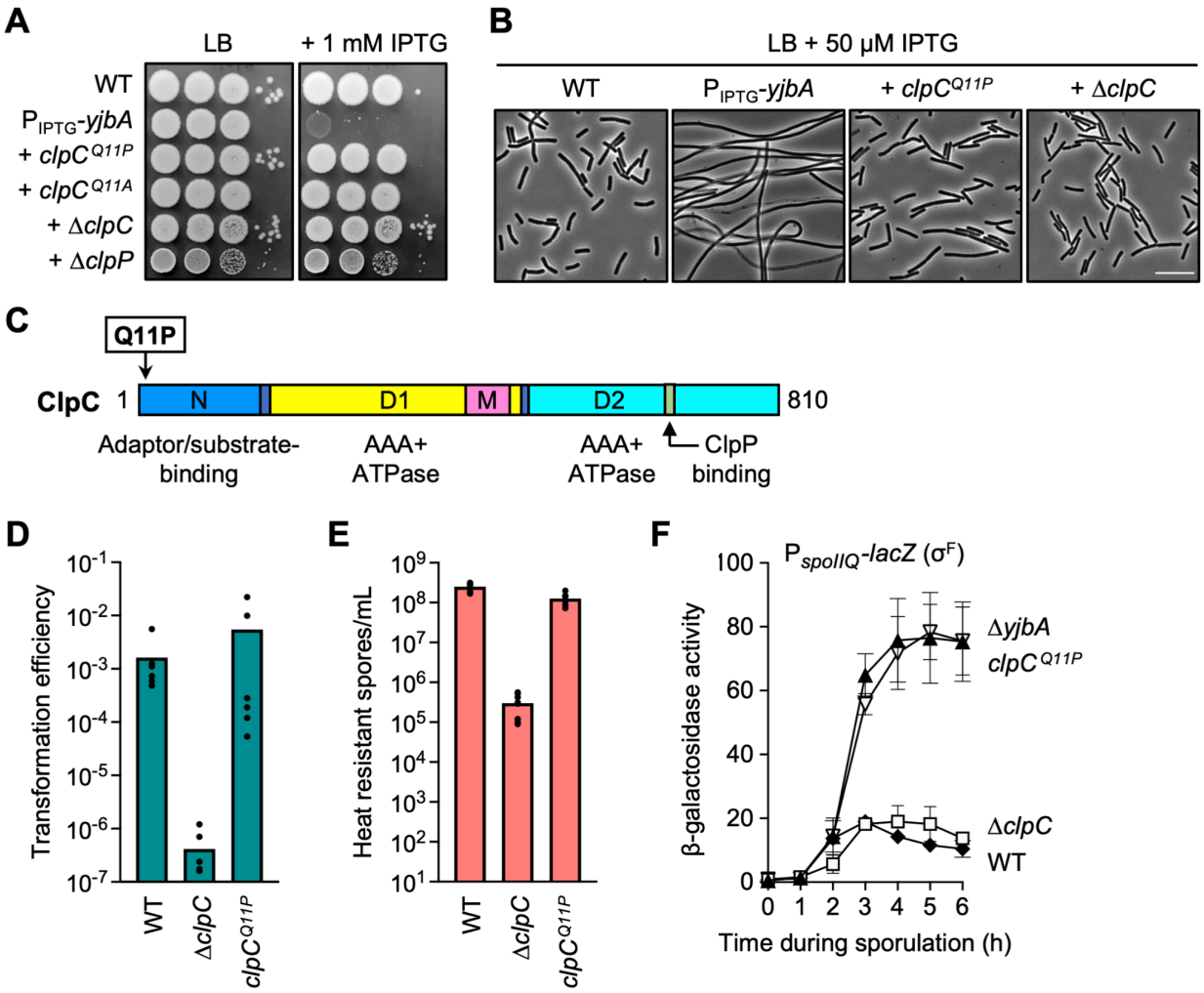

Figure 2. The *clpC*^{Q11P} allele suppresses vegetative *yjbA* toxicity and, like Δ*yjbA*, stimulates σ^F activity during sporulation.

(A) Expression of *yjbA* during vegetative growth causes cell death at high inducer concentrations, and this toxicity is suppressed by mutations in *clpC* and *clpP*. Wild type cells and cells harboring an engineered IPTG-inducible *yjbA* gene construct (WT and P_{IPTG}-*yjbA*; strains PY79 and CFB189, respectively), as well as P_{IPTG}-*yjbA* cells harboring *clpC*^{Q11P}, *clpC*^{Q11A}, Δ*clpC*, or Δ*clpP* (strains SFB32, SFB38, CFB241, and CFB274, respectively), were grown to mid-logarithmic phase (OD_{600}~0.5) in LB media, adjusted to OD_{600}=1, and 10-fold serial dilutions (10^{-1}-10^{-4}, left to right) were spotted onto LB plates with or without 1 mM IPTG. Plates were imaged after 24 h of growth at 37°C.

(B) Expression of *yjbA* during vegetative growth causes cell filamentation at lower inducer concentrations, and this filamentation is suppressed by *clpC*^{Q11P} and Δ*clpC*. WT, P_{IPTG}-*yjbA*, P_{IPTG}-*yjbA clpC*^{Q11P}, and P_{IPTG}-*yjbA* Δ*clpC* cells (strains PY79, CFB189, SMB361, and CFB241, respectively) were grown for ~24 h at 37°C on LB agar plates with 50 μM IPTG. Colonies were picked, diluted, and visualized by phase microscopy. Scale bar, 10 μm.

(C) Domain structure of the ClpC protein. Shown are the adaptor/substrate-binding N domain (blue), AAA+ ATPase D1 domain (yellow), M-domain (magenta), and AAA+ ATPase D2 domain (cyan). The ClpP binding site within the D2 domain is also indicated in green. The location of the Q11P substitution, one of several isolated suppressors of vegetative *yjbA* toxicity, is labeled.
(D) Cells harboring the *clpC*^{Q11P} allele, unlike those harboring Δ*clpC*, do not have a competence defect. Transformation efficiency for WT, Δ*clpC*, and *clpC*^{Q11P} cells (strains PY79, CFB270 and CFB282, respectively) was calculated by dividing the number of colonies that acquired spectinomycin resistance from plasmid pDG1730 by the total number of viable colonies after transformation. Individual data points are shown (n=6) and bars indicate the mean transformation efficiency for each strain.
(E) Cells harboring the *clpC*^{Q11P} allele, unlike those harboring Δ*clpC*, do not have a severe sporulation defect. WT, Δ*clpC*, and *clpC*^{Q11P} cells (strains PY79, CFB270 and CFB282, respectively) were induced to sporulate for 24 h and the number of heat resistant spores per mL were determined. Individual data points are shown (n=6) and bars indicate the mean transformation efficiency for each strain.
(F) The *clpC*^{Q11P} allele, like Δ*yjbA* but unlike Δ*clpC*, significantly stimulates σ^F activity during sporulation. β-Galactosidase production from the σ^F-dependent P_{spoIIQ}-*lacZ* reporter was monitored during sporulation of otherwise wild type cells (WT; closed diamonds), cells deleted for *yjbA* (Δ*yjbA*; open inverted triangles), cells deleted for *clpC* (Δ*clpC*; open squares) or cells harboring *clpC*^{Q11P} (*clpC*^{Q11P}; solid triangles) (strains AHB881, SMB189, CFB302, and CFB307, respectively). Error bars indicate ± standard deviations based on four replicates.

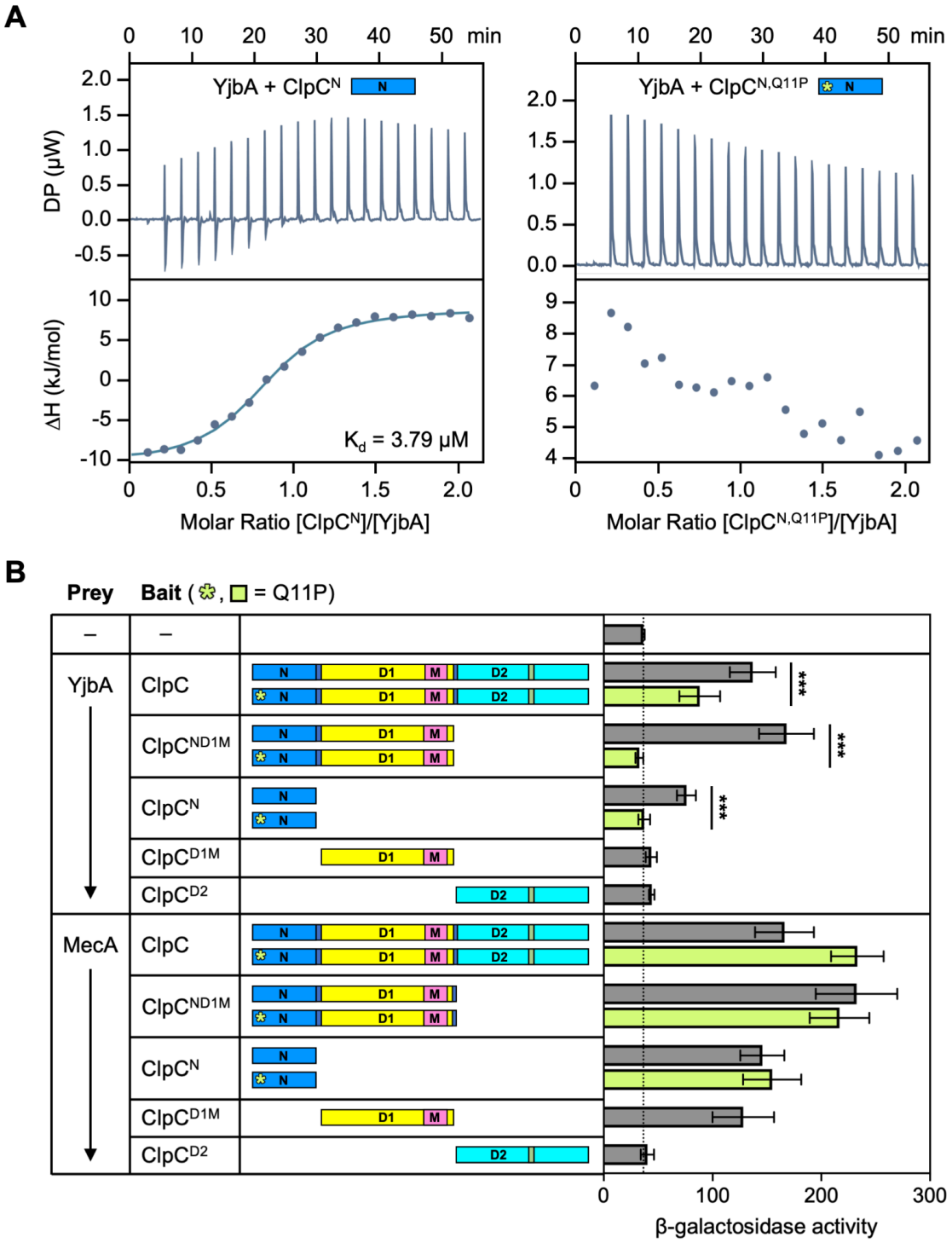

Figure 3. YjbA interacts with the ClpC N-domain in a Gln11-dependent manner.
(A) Isothermal titration calorimetry (ITC) experiments indicate that YjbA and $ClpC^{N}$ (left), but not YjbA and $ClpC^{N,Q11P}$ (right) form a complex *in vitro*. Twenty injections of 2 µl YjbA at a concentration of 700 µM were added to ClpC constructs at 70 µM in the reaction cell. The heat

of YjbA dilution into buffer was subtracted from the data. Raw data is shown in upper panels, binding isotherm in lower panels. Fitted data for YjbA-$ClpC^N$ interaction: $\Delta H = -19.5 \pm 0.6$ kJ/mol; $K_D = 3.79 \pm 0.50$ μM; N = 0.82 ± 0.01 sites.
(B) YjbA and ClpC interact in a bacterial two-hybrid assay in a manner that depends upon the ClpC N-domain and Gln11. In this assay, interaction of "Bait" and "Prey" proteins, fused respectively to the bacteriophage λ cI protein (λcI) and the N-terminal domain of the α subunit of RNA polymerase (α), drives expression of a *lacZ* reporter gene under the control of a test promoter in *E. coli*, leading to production of β-galactosidase (Dove et al. 1997). ClpC or variants thereof were expressed from plasmids as fusions to λcI ("Bait"), while YjbA or the well-characterized ClpC adaptor protein MecA were expressed as fusions to α ("Prey"). The full list of bacterial two hybrid plasmids is provided in **Supplemental Table S2** and the resulting bacterial two hybrid strains are listed in **Supplemental Table S6**. Variants of ClpC ($ClpC^{ND1M}$, $ClpC^N$, $ClpC^{D1M}$, and $ClpC^{D2}$) harboring one or more of its domains and/or the Q11P substitution are depicted in a manner derived from **Fig 2C**. The Q11P substitution is indicated by a pale green asterisk, and data collected from pairs including a ClpC Q11P variant are shaded pale green. The dotted line represents background β-galactosidase activity in a negative control strain expressing λCI and the α subunit of RNA polymerase alone (depicted as "–" for both prey and bait). Data are plotted as mean values, with error bars indicating ± standard deviation (n=5-18 replicate values). ***$p < 0.0001$, unpaired *t* test with Welch's correction.

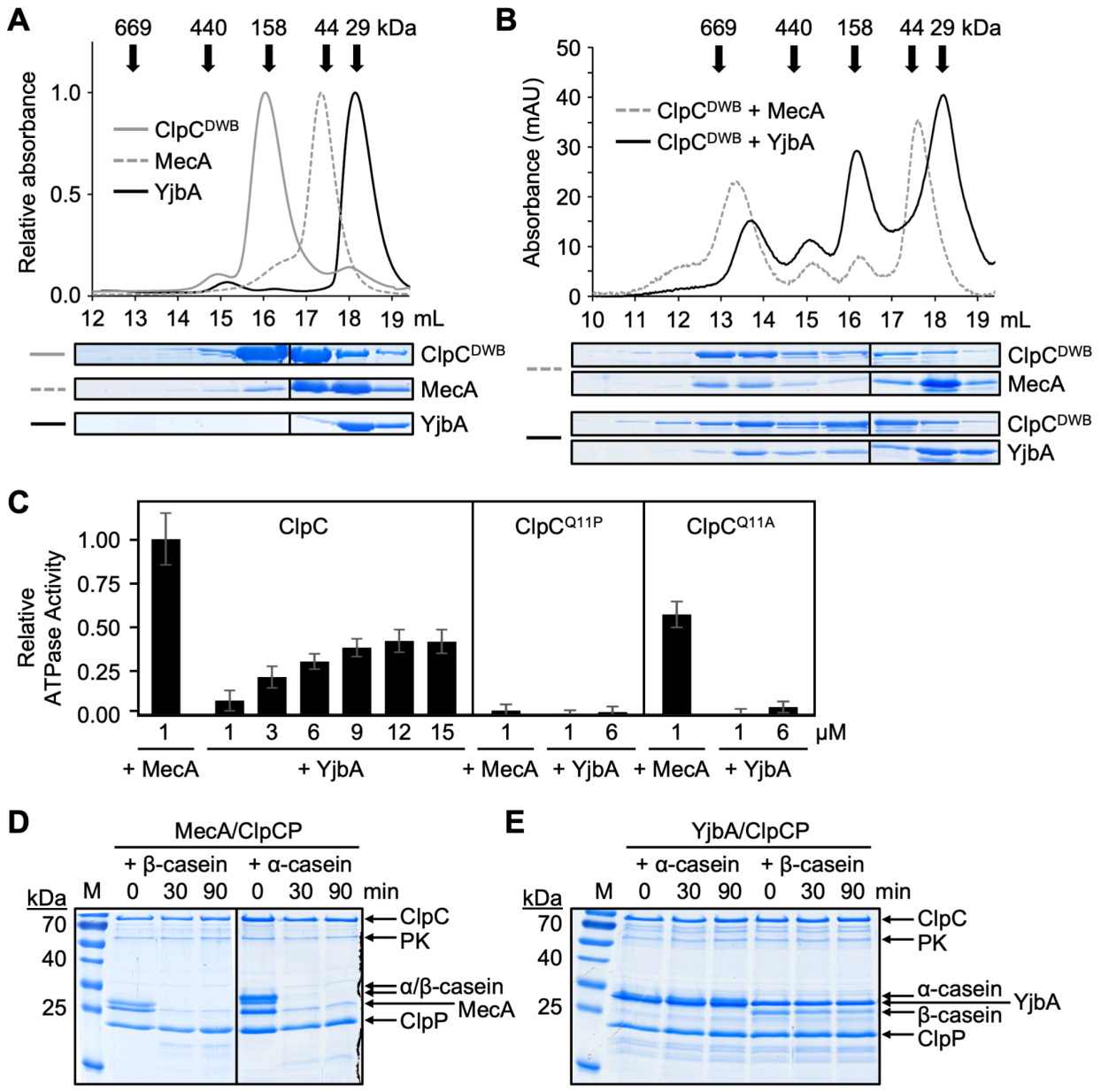

Figure 4. YjbA induces oligomerization and ATPase activity of full-length ClpC *in vitro*, but does not direct degradation of a test substrate.

(A,B) Like MecA, YjbA induces the formation of stable higher oligomeric complexes with a ClpC double Walker B variant ($ClpC^{DWB}$) in the presence of ATP, as detected by size exclusion chromatography. The elution profiles of all proteins **(A)** alone and **(B)** in combinations (as indicated; 10 μM each) were detected by absorbance at 280 nm. The positions and molecular weights of native marker proteins are indicated with black arrows. Elution fractions were

concentrated and analyzed by SDS-PAGE followed by Coomassie staining, the results of which are shown below each relevant fraction.

(C) Like MecA, YjbA induces the ATPase activity of ClpC. The ATPase activity of ClpC, $ClpC^{Q11P}$, or $ClpC^{Q11A}$ (1 μM each) was determined in the presence of MecA (1 μM) or YjbA (1-15 μM, as indicated). All ATPase activities were normalized to that of ClpC induced by MecA. Error bars indicate ± standard deviations based on at least three replicates.

(D,E) Unlike MecA, YjbA does not induce ClpCP-mediated degradation of α/β-casein. Samples from *in vitro* degradation reactions harboring the indicated proteins (1 μM each) as well as an ATP regeneration system (pyruvate kinase [PK]) were taken at 0, 30, and 90 min and analyzed by SDS-PAGE followed by Coomassie staining.

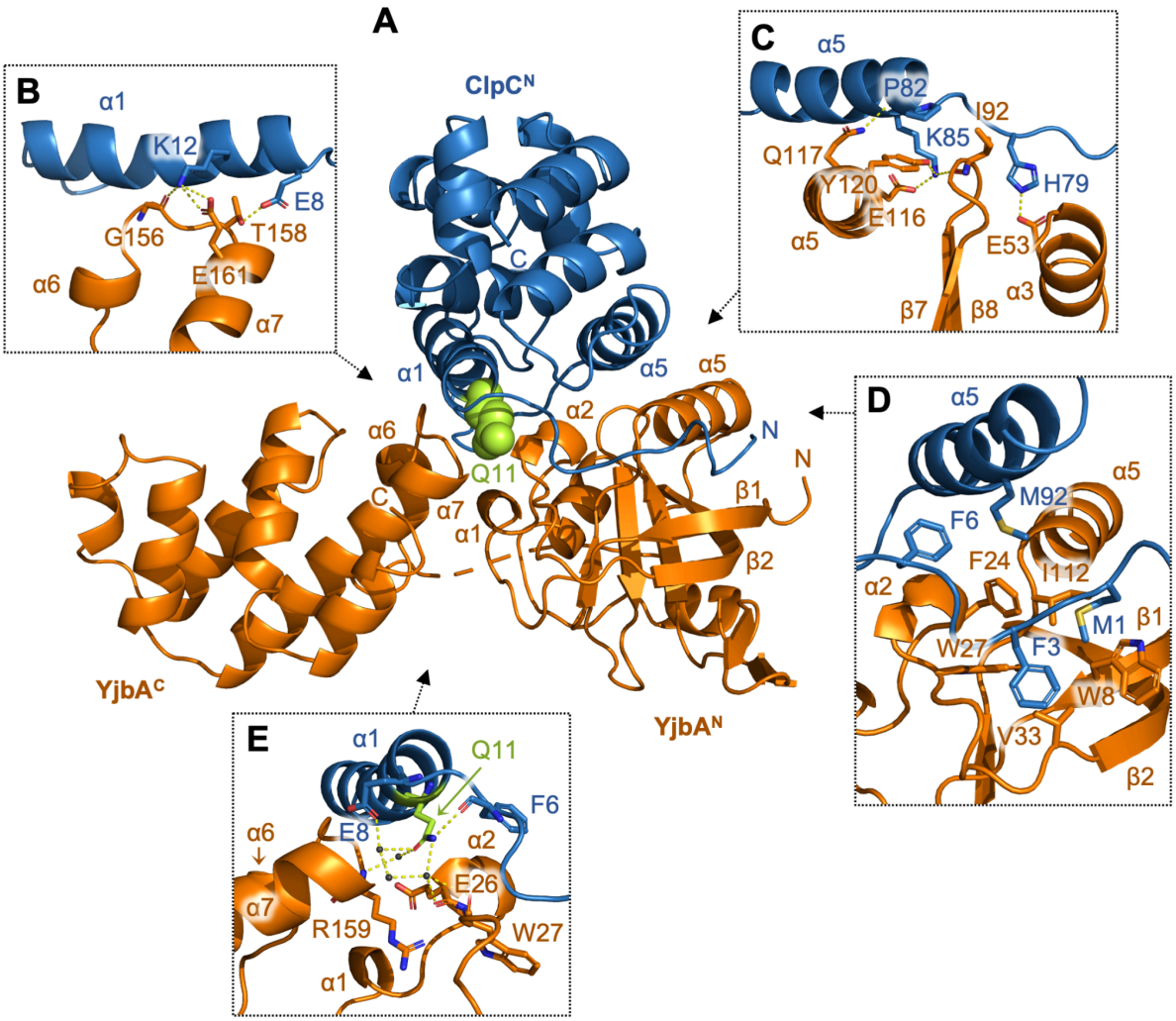

Figure 5. A co-crystal structure of ClpC^N and YjbA.
(A) Complete X-ray crystal structure of YjbA (gold) in complex with ClpC^N (blue) with Gln11 highlighted (lime green space fill) solved to 2.0 Å resolution.
(B-C) Zoomed views highlighting hydrogen bonding patterns between: **(B)** Helix 1 of ClpC^N and the loop between helices 6 and 7 of YjbA; **(C)** Helix 5 of ClpC^N and helix 5, the end of helix 3 and the beta hairpin of YjbA.
(D) Zoomed view of hydrophobic interactions between ClpC^N and YjbA^N.
(E) Zoomed view of interaction network surrounding Gln11, mediated via water molecules.

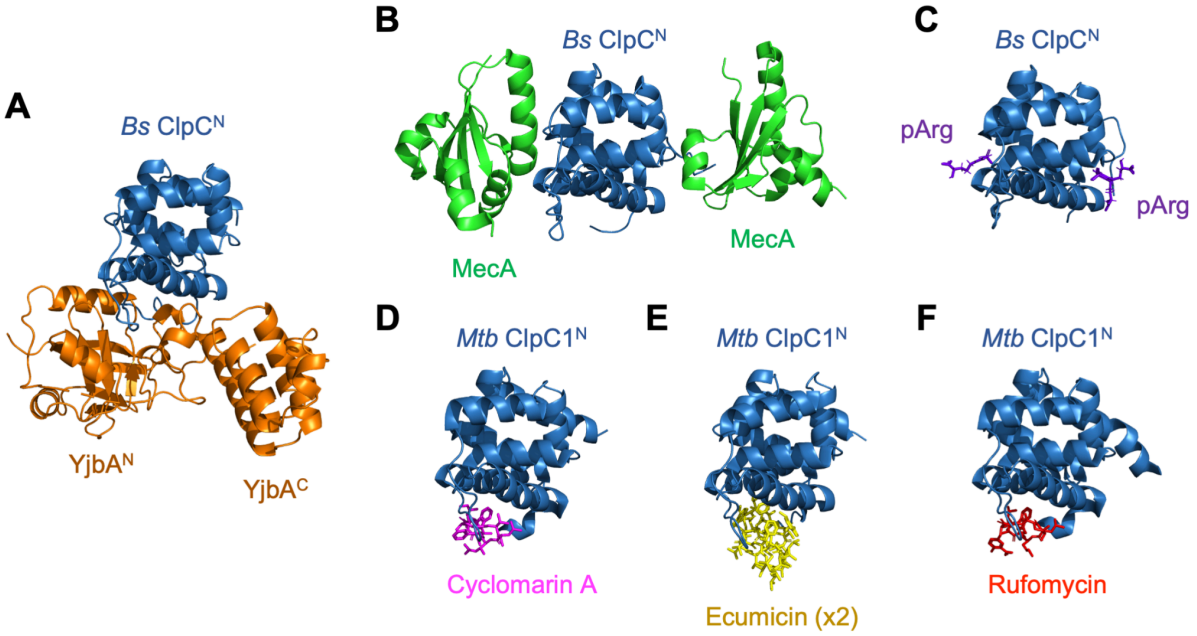

Figure 6. YjbA binds ClpC^N in a location distinct from that bound by the *B. subtilis* ClpC adaptor MecA and phosphoarginine (pArg) peptides, but similar to the surface of *M. tuberculosis* ClpC1^N bound by the antibiotics Cyclomarin A, Ecumicin, and Rufomycin.
(A-C) Co-crystal structures of the *B. subtilis* ClpC N-domain bound to **(A)** YjbA (PDB: 8B3S; this study), **(B)** MecA (PDB: 3PXG) (Wang et al. 2011), and **(C)** phosphoarginine (pArg; PDB: 5HBN) (Trentini et al. 2016).
(D-F) Co-crystal structures of the *M. tuberculosis* ClpC N-domain bound to **(D)** cyclomarin A (PDB: 3WDC) (Vasudevan et al. 2013), **(E)** ecumicin (PDB: 6PBS) (Wolf et al. 2020), and **(F)** rufomycin (PDB: 6CN8) (Wolf et al. 2019).

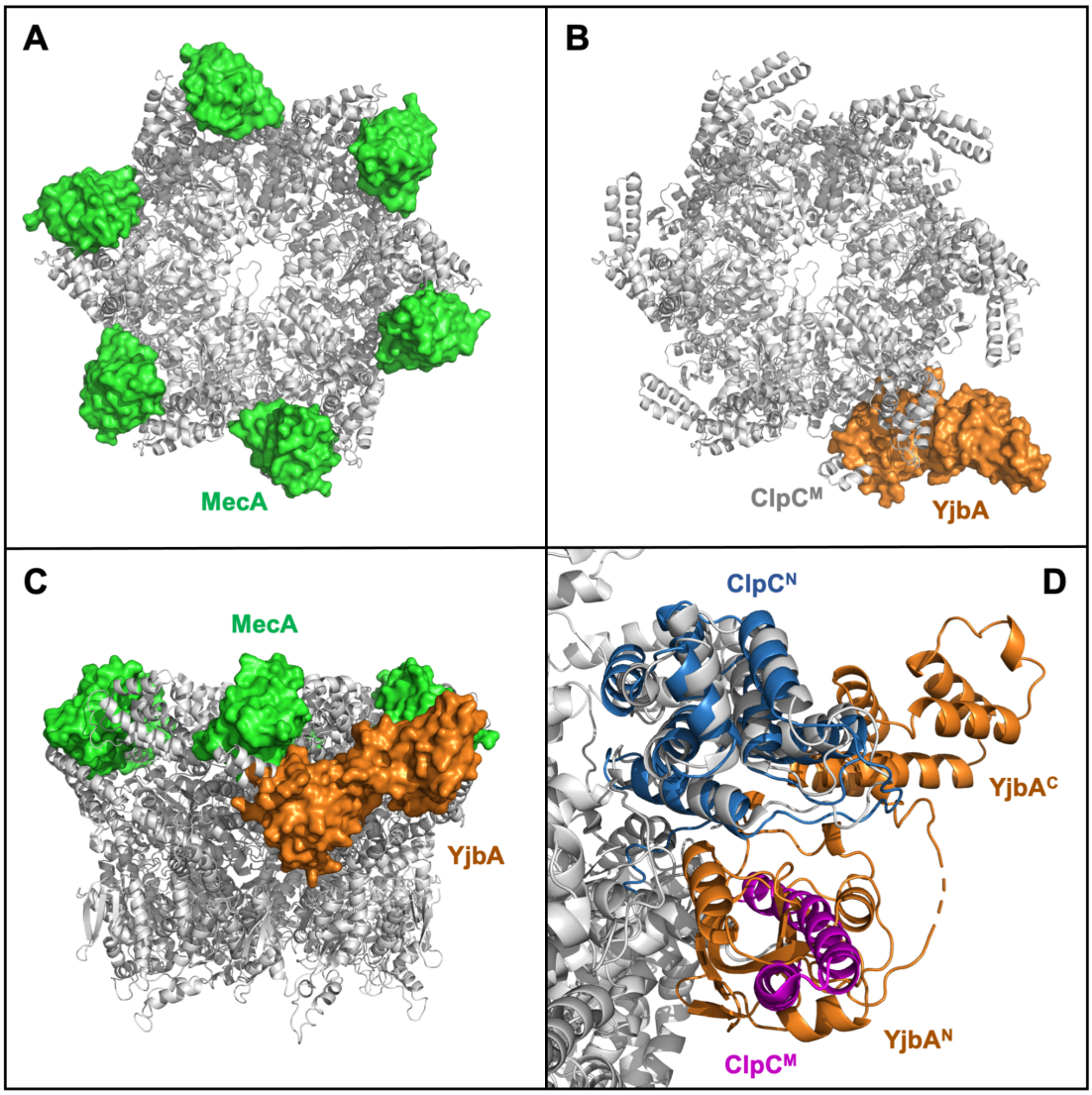

Figure 7. Modeling YjbA onto the ClpC hexamer indicates potential steric clash with the ClpC M-domain

(A) Co-crystal structure (PDB: 3J3T) of *B. subtilis* MecA (green) in a hexameric complex with ClpC (gray) (Liu et al. 2013). **(B,C,D)** Alternate views of the YjbA/ClpC^{N} crystal complex (PDB: 8B3S, this work) aligned with ClpC^{N} in the full length ClpC hexamer shown in (A), indicating that YjbA (orange) and MecA (green) occupy different binding positions on ClpC^{N} **(D)** Zoomed view showing the steric clash between YjbA (orange) and the ClpC M-domain (magenta). The overlay of ClpC^{N} from the hexamer (gray) and the YjbA/ClpC^{N} co-crystal structure (blue) is shown in (D) but removed from images (B) and (C) for clarity.

ACKNOWLEDGEMENTS

This work was funded by grants from the National Institutes of Health (NIH) (DP2 GM105439 to AHC), the Biotechnology and Biological Sciences Research Council (BBSRC) (BB/N006267/1, BB/R006091/1, BB/S006877/1, and BB/X001415/1 to RLI), the Max Planck Society & Deutsche Forschungsgemeinschaft (Tu106/6 and Tu106/8 [SPP1879] to KT), and a Ph.D. fellowship from the Hannover School for Biomolecular Drug Research (HSBDR) (to IH). The authors would like to thank Diamond Light Source for beamtime (proposal mx13597; King's College London BAG). NMR experiments were performed at the Centre for Biomolecular Spectroscopy, King's College London, established with a Capital Award from the Wellcome Trust. This work was also supported by the Francis Crick Institute through provision of access to the MRC Biomedical NMR Centre. The Francis Crick Institute received core funding from Cancer Research UK (FC001029), the UK Medical Research Council (FC001029), and the Wellcome Trust (FC001029). The 950 MHz NMR facility at the University of Oxford was funded by the Wellcome Trust Joint Infrastructure Fund and the E. P. Abraham Fund.

REFERENCES CITED

Altschul SF, Gish W, Miller W, Myers EW, Lipman DJ. 1990. Basic local alignment search tool. *J Mol Biol* **215**: 403–410.

Arrieta-Ortiz ML, Hafemeister C, Bate AR, Chu T, Greenfield A, Shuster B, Barry SN, Gallitto M, Liu B, Kacmarczyk T, et al. 2015. An experimentally supported model of the *Bacillus subtilis* global transcriptional regulatory network. *Mol Syst Biol* **11**: 839–839.

Bard JAM, Goodall EA, Greene ER, Jonsson E, Dong KC, Martin A. 2018. Structure and function of the 26S proteasome. *Annu Rev Biochem* **87**: 697–724.

Biørnstad TJ, Håvarstein LS. 2011. ClpC acts as a negative regulator of competence in *Streptococcus thermophilus*. *Microbiol Read Engl* **157**: 1676–1684.

Birk MS, Ahmed-Begrich R, Tran S, Elsholz AKW, Frese CK, Charpentier E. 2021. Time-resolved proteome analysis of *Listeria monocytogenes* during infection reveals the

role of the AAA+ chaperone ClpC for host cell adaptation. *mSystems* **6**: e0021521.

Bradshaw N, Losick R. 2015. Asymmetric division triggers cell-specific gene expression through coupled capture and stabilization of a phosphatase. *eLife* **4**: e08145.

Camp AH, Losick R. 2009. A feeding tube model for activation of a cell-specific transcription factor during sporulation in *Bacillus subtilis*. *Genes Dev* **23**: 1014–1024.

Carroni M, Franke KB, Maurer M, Jäger J, Hantke I, Gloge F, Linder D, Gremer S, Turgay K, Bukau B, et al. 2017. Regulatory coiled-coil domains promote head-to-head assemblies of AAA+ chaperones essential for tunable activity control. *eLife* **6**: e30120.

Choules MP, Wolf NM, Lee H, Anderson JR, Grzelak EM, Wang Y, Ma R, Gao W, McAlpine JB, Jin Y-Y, et al. 2019. Rufomycin targets ClpC1 proteolysis in *Mycobacterium tuberculosis* and *M. abscessus*. *Antimicrob Agents Chemother* **63**.

Collins GA, Goldberg AL. 2017. The logic of the 26S proteasome. *Cell* **169**: 792–806.

Culp E, Wright GD. 2017. Bacterial proteases, untapped antimicrobial drug targets. *J Antibiot (Tokyo)* **70**: 366–377.

de Hoon MJL, Eichenberger P, Vitkup D. 2010. Hierarchical evolution of the bacterial sporulation network. *Curr Biol* **20**: R735-45.

Deaconescu AM, Chambers AL, Smith AJ, Nickels BE, Hochschild A, Savery NJ, Darst SA. 2006. Structural basis for bacterial transcription-coupled DNA repair. *Cell* **124**: 507–520.

Deuerling E, Mogk A, Richter C, Purucker M, Schumann W. 1997. The *ftsH* gene of *Bacillus subtilis* is involved in major cellular processes such as sporulation, stress adaptation and secretion. *Mol Microbiol* **23**: 921–933.

Dove SL, Hochschild A. 2004. A bacterial two-hybrid system based on transcription activation. *Methods Mol Biol Clifton NJ* **261**: 231–246.

Dove SL, Joung JK, Hochschild A. 1997. Activation of prokaryotic transcription through arbitrary protein-protein contacts. *Nature* **386**: 627–630.

Evans R, O'Neill M, Pritzel A, Antropova N, Senior A, Green T, Žídek A, Bates R, Blackwell S, Yim J, et al. 2022. Protein complex prediction with AlphaFold-Multimer. 2021.10.04.463034. https://www.biorxiv.org/content/10.1101/2021.10.04.463034v2 (Accessed January 9, 2023).

Fricker LD. 2020. Proteasome inhibitor drugs. *Annu Rev Pharmacol Toxicol* **60**: 457–476.

Fujita M, Losick R. 2002. An investigation into the compartmentalization of the sporulation transcription factor σ^E in *Bacillus subtilis*. *Mol Microbiol* **43**: 27–38.

Gao W, Kim J-Y, Anderson JR, Akopian T, Hong S, Jin Y-Y, Kandror O, Kim J-W, Lee I-A, Lee S-Y, et al. 2015. The cyclic peptide ecumicin targeting ClpC1 is active against *Mycobacterium tuberculosis in vivo*. *Antimicrob Agents Chemother* **59**: 880–889.

Gavrish E, Sit CS, Cao S, Kandror O, Spoering A, Peoples A, Ling L, Fetterman A, Hughes D, Bissell A, et al. 2014. Lassomycin, a ribosomally synthesized cyclic peptide, kills *Mycobacterium tuberculosis* by targeting the ATP-dependent protease ClpC1P1P2. *Chem Biol* **21**: 509–518.

Gerth U, Krüger E, Derré I, Msadek T, Hecker M. 1998. Stress induction of the *Bacillus subtilis clpP* gene encoding a homologue of the proteolytic component of the Clp protease and the involvement of ClpP and ClpX in stress tolerance. *Mol Microbiol* **28**: 787–802.

Goldberg AL. 2012. Development of proteasome inhibitors as research tools and cancer drugs. *J Cell Biol* **199**: 583–588.

Gueiros-Filho FJ, Losick R. 2002. A widely conserved bacterial cell division protein that promotes assembly of the tubulin-like protein FtsZ. *Genes Dev* **16**: 2544–2556.

Guérout-Fleury AM, Frandsen N, Stragier P. 1996. Plasmids for ectopic integration in *Bacillus subtilis*. *Gene* **180**: 57–61.

Gunaratnam G, Tuchscherr L, Elhawy MI, Bertram R, Eisenbeis J, Spengler C, Tschernig T, Löffler B, Somerville GA, Jacobs K, et al. 2019. ClpC affects the intracellular survival capacity of *Staphylococcus aureus* in non-professional phagocytic cells. *Sci Rep* **9**: 16267.

Haeusser DP, Margolin W. 2016. Splitsville: structural and functional insights into the dynamic bacterial Z ring. *Nat Rev Microbiol* **14**: 305–319.

Hands-Taylor KLD, Martino L, Tata R, Babon JJ, Bui TT, Drake AF, Beavil RL, Pruijn GJM, Brown PR, Conte MR. 2010. Heterodimerization of the human RNase P/MRP subunits Rpp20 and Rpp25 is a prerequisite for interaction with the P3 arm of RNase MRP RNA. *Nucleic Acids Res* **38**: 4052–4066.

Holm L, Laakso LM. 2016. Dali server update. *Nucleic Acids Res* **44**: W351-5.

Ju J, Luo T, Haldenwang WG. 1998. Forespore expression and processing of the SigE transcription factor in wild-type and mutant *Bacillus subtilis*. *J Bacteriol* **180**: 1673–1681.

Jumper J, Evans R, Pritzel A, Green T, Figurnov M, Ronneberger O, Tunyasuvunakool K, Bates R, Žídek A, Potapenko A, et al. 2021. Highly accurate protein structure prediction with AlphaFold. *Nature* **596**: 583–589.

Kain J, He GG, Losick R. 2008. Polar localization and compartmentalization of ClpP proteases

during growth and sporulation in *Bacillus subtilis*. *J Bacteriol* **190**: 6749–6757.

Käll L, Krogh A, Sonnhammer ELL. 2005. An HMM posterior decoder for sequence feature prediction that includes homology information. *Bioinformatics* **21 Suppl 1**: i251-7.

Kirstein J, Schlothauer T, Dougan DA, Lilie H, Tischendorf G, Mogk A, Bukau B, Turgay K. 2006. Adaptor protein controlled oligomerization activates the AAA+ protein ClpC. *EMBO J* **25**: 1481–1491.

Kojetin DJ, McLaughlin PD, Thompson RJ, Dubnau D, Prepiak P, Rance M, Cavanagh J. 2009. Structural and motional contributions of the *Bacillus subtilis* ClpC N-domain to adaptor protein interactions. *J Mol Biol* **387**: 639–652.

Krissinel E, Henrick K. 2004. Secondary-structure matching (SSM), a new tool for fast protein structure alignment in three dimensions. *Acta Crystallogr D Biol Crystallogr* **60**: 2256–2268.

Krüger E, Völker U, Hecker M. 1994. Stress induction of *clpC* in *Bacillus subtilis* and its involvement in stress tolerance. *J Bacteriol* **176**: 3360–3367.

Kuhlmann NJ, Chien P. 2017. Selective adaptor dependent protein degradation in bacteria. *Curr Opin Microbiol* **36**: 118–127.

Lanzetta PA, Alvarez LJ, Reinach PS, Candia OA. 1979. An improved assay for nanomole amounts of inorganic phosphate. *Anal Biochem* **100**: 95–97.

Le ATT, Schumann W. 2009. The Spo0E phosphatase of *Bacillus subtilis* is a substrate of the FtsH metalloprotease. *Microbiol Read Engl* **155**: 1122–1132.

Liu J, Cosby WM, Zuber P. 1999. Role of Lon and ClpX in the post-translational regulation of a sigma subunit of RNA polymerase required for cellular differentiation in *Bacillus subtilis*. *Mol Microbiol* **33**: 415–428.

Liu J, Mei Z, Li N, Qi Y, Xu Y, Shi Y, Wang F, Lei J, Gao N. 2013. Structural dynamics of the MecA-ClpC complex: a type II AAA+ protein unfolding machine. *J Biol Chem* **288**: 17597–17608.

Magnin T, Lord M, Yudkin MD. 1997. Contribution of partner switching and SpoIIAA cycling to regulation of σ^F activity in sporulating *Bacillus subtilis*. *J Bacteriol* **179**: 3922–3927.

Mahmoud SA, Chien P. 2018. Regulated proteolysis in bacteria. *Annu Rev Biochem* **87**: 677–696.

Marchler-Bauer A, Bo Y, Han L, He J, Lanczycki CJ, Lu S, Chitsaz F, Derbyshire MK, Geer RC, Gonzales NR, et al. 2017. CDD/SPARCLE: functional classification of proteins via subfamily domain architectures. *Nucleic Acids Res* **45**: D200–D203.

Mashruwala AA, Eilers BJ, Fuchs AL, Norambuena J, Earle CA, van de Guchte A, Tripet BP, Copié V, Boyd JM. 2019. The ClpCP complex modulates respiratory metabolism in *Staphylococcus aureus* and is regulated in a SrrAB-dependent manner. *J Bacteriol* **201**.

Maurer M, Linder D, Franke KB, Jäger J, Taylor G, Gloge F, Gremer S, Le Breton L, Mayer MP, Weber-Ban E, et al. 2019. Toxic activation of an AAA+ protease by the antibacterial drug Cyclomarin A. *Cell Chem Biol* **26**: 1169-1179.e4.

Meeske AJ, Rodrigues CDA, Brady J, Lim HC, Bernhardt TG, Rudner DZ. 2016. High-throughput genetic screens identify a large and diverse collection of new sporulation genes in *Bacillus subtilis*. *PLoS Biol* **14**: e1002341.

Mogk A, Dougan D, Weibezahn J, Schlieker C, Turgay K, Bukau B. 2004. Broad yet high substrate specificity: the challenge of AAA+ proteins. *J Struct Biol* **146**: 90–98.

Morlot C, Rodrigues CDA. 2018. The new kid on the block: A specialized secretion system during bacterial sporulation. *Trends Microbiol* **26**: 663–676.

Morreale FE, Kleine S, Leodolter J, Junker S, Hoi DM, Ovchinnikov S, Okun A, Kley J, Kurzbauer R, Junk L, et al. 2022. BacPROTACs mediate targeted protein degradation in bacteria. *Cell* S0092-8674(22)00593–1.

Msadek T, Dartois V, Kunst F, Herbaud ML, Denizot F, Rapoport G. 1998. ClpP of *Bacillus subtilis* is required for competence development, motility, degradative enzyme synthesis, growth at high temperature and sporulation. *Mol Microbiol* **27**: 899–914.

Msadek T, Kunst F, Rapoport G. 1994. MecB of *Bacillus subtilis*, a member of the ClpC ATPase family, is a pleiotropic regulator controlling competence gene expression and growth at high temperature. *Proc Natl Acad Sci U S A* **91**: 5788–5792.

Nanamiya H, Ohashi Y, Asai K, Moriya S, Ogasawara N, Fujita M, Sadaie Y, Kawamura F. 1998. ClpC regulates the fate of a sporulation initiation sigma factor, σ^H protein, in *Bacillus subtilis* at elevated temperatures. *Mol Microbiol* **29**: 505–513.

Nicholson WL, Setlow P. 1990. Sporulation, germination and outgrowth. In *Molecular Biology Methods for* Bacillus (eds. C.R. Harwood and S.M. Cutting), pp. 391–450, John Wiley & Sons Ltd., New York City, NY.

Pan Q, Garsin DA, Losick R. 2001. Self-reinforcing activation of a cell-specific transcription factor by proteolysis of an anti-σ factor in *B. subtilis*. *Mol Cell* **8**: 873–883.

Pan Q, Losick R. 2003. Unique degradation signal for ClpCP in *Bacillus subtilis*. *J Bacteriol* **185**: 5275–5278.

Park Y-H, Jeong MS, Jang SB. 2016. Structural insights of homotypic interaction domains in the

ligand-receptor signal transduction of tumor necrosis factor (TNF). *BMB Rep* **49**: 159–166.

Raju RM, Goldberg AL, Rubin EJ. 2012. Bacterial proteolytic complexes as therapeutic targets. *Nat Rev Drug Discov* **11**: 777–789.

Riley EP, Lopez-Garrido J, Sugie J, Liu RB, Pogliano K. 2021. Metabolic differentiation and intercellular nurturing underpin bacterial endospore formation. *Sci Adv* **7**: eabd6385.

Riley EP, Schwarz C, Derman AI, Lopez-Garrido J. 2020. Milestones in *Bacillus subtilis* sporulation research. *Microb Cell Graz Austria* **8**: 1–16.

Rouquette C, de Chastellier C, Nair S, Berche P. 1998. The ClpC ATPase of *Listeria monocytogenes* is a general stress protein required for virulence and promoting early bacterial escape from the phagosome of macrophages. *Mol Microbiol* **27**: 1235–1245.

Ruvolo MV, Mach KE, Burkholder WF. 2006. Proteolysis of the replication checkpoint protein Sda is necessary for the efficient initiation of sporulation after transient replication stress in *Bacillus subtilis*. *Mol Microbiol* **60**: 1490–1508.

Sauer RT, Baker TA. 2011. AAA+ proteases: ATP-fueled machines of protein destruction. *Annu Rev Biochem* **80**: 587–612.

Schaeffer P, Millet J, Aubert JP. 1965. Catabolic repression of bacterial sporulation. *Proc Natl Acad Sci U S A* **54**: 704–711.

Schlothauer T, Mogk A, Dougan DA, Bukau B, Turgay K. 2003. MecA, an adaptor protein necessary for ClpC chaperone activity. *Proc Natl Acad Sci U S A* **100**: 2306–2311.

Schmitt EK, Riwanto M, Sambandamurthy V, Roggo S, Miault C, Zwingelstein C, Krastel P, Noble C, Beer D, Rao SPS, et al. 2011. The natural product cyclomarin kills *Mycobacterium tuberculosis* by targeting the ClpC1 subunit of the caseinolytic protease. *Angew Chem Int Ed* **50**: 5889–5891.

Serrano M, Hövel S, Moran CP, Henriques AO, Völker U. 2001. Forespore-specific transcription of the *lonB* gene during sporulation in *Bacillus subtilis*. *J Bacteriol* **183**: 2995–3003.

Sierro N, Makita Y, de Hoon M, Nakai K. 2008. DBTBS: a database of transcriptional regulation in *Bacillus subtilis* containing upstream intergenic conservation information. *Nucleic Acids Res* **36**: D93-6.

Steil L, Serrano M, Henriques AO, Völker U. 2005. Genome-wide analysis of temporally regulated and compartment-specific gene expression in sporulating cells of *Bacillus subtilis*. *Microbiol Read Engl* **151**: 399–420.

Sterlini JM, Mandelstam J. 1969. Commitment to sporulation in *Bacillus subtilis* and its

relationship to development of actinomycin resistance. *Biochem J* **113**: 29–37.

Tan IS, Ramamurthi KS. 2014. Spore formation in *Bacillus subtilis*. *Environ Microbiol Rep* **6**: 212–225.

Tan IS, Weiss CA, Popham DL, Ramamurthi KS. 2015. A quality-control mechanism removes unfit cells from a population of sporulating bacteria. *Dev Cell* **34**: 682–693.

Taylor G, Frommherz Y, Katikaridis P, Layer D, Sinning I, Carroni M, Weber-Ban E, Mogk A. 2022. Antibacterial peptide CyclomarinA creates toxicity by deregulating the *Mycobacterium tuberculosis* ClpC1-ClpP1P2 protease. *J Biol Chem* **298**: 102202.

Trentini DB, Suskiewicz MJ, Heuck A, Kurzbauer R, Deszcz L, Mechtler K, Clausen T. 2016. Arginine phosphorylation marks proteins for degradation by a Clp protease. *Nature* **539**: 48–53.

Tung C-H, Huang J-W, Yang J-M. 2007. Kappa-alpha plot derived structural alphabet and BLOSUM-like substitution matrix for rapid search of protein structure database. *Genome Biol* **8**: R31.

Turgay K, Hahn J, Burghoorn J, Dubnau D. 1998. Competence in *Bacillus subtilis* is controlled by regulated proteolysis of a transcription factor. *EMBO J* **17**: 6730–6738.

Turgay K, Hamoen LW, Venema G, Dubnau D. 1997. Biochemical characterization of a molecular switch involving the heat shock protein ClpC, which controls the activity of ComK, the competence transcription factor of *Bacillus subtilis*. *Genes Dev* **11**: 119–128.

Vasudevan D, Rao SPS, Noble CG. 2013. Structural basis of mycobacterial inhibition by cyclomarin A. *J Biol Chem* **288**: 30883–30891.

Wang F, Mei Z, Qi Y, Yan C, Hu Q, Wang J, Shi Y. 2011. Structure and mechanism of the hexameric MecA-ClpC molecular machine. *Nature* **471**: 331–335.

Wang ST, Setlow B, Conlon EM, Lyon JL, Imamura D, Sato T, Setlow P, Losick R, Eichenberger P. 2006. The forespore line of gene expression in *Bacillus subtilis*. *J Mol Biol* **358**: 16–37.

Wilson GA, Bott KF. 1968. Nutritional factors influencing the development of competence in the *Bacillus subtilis* transformation system. *J Bacteriol* **95**: 1439–1449.

Wolf NM, Lee H, Choules MP, Pauli GF, Phansalkar R, Anderson JR, Gao W, Ren J, Santarsiero BD, Lee H, et al. 2019. High-resolution structure of ClpC1-rufomycin and ligand binding studies provide a framework to design and optimize anti-tuberculosis leads. *ACS Infect Dis* **5**: 829–840.

Wolf NM, Lee H, Zagal D, Nam JW, Oh DC, Lee H, Suh JW, Pauli GF, Cho S, Abad-Zapatero C. 2020. Structure of the N-terminal domain of ClpC1 in complex with the antituberculosis

natural product ecumicin reveals unique binding interactions. *Acta Crystallogr Sect Struct Biol* **76**: 458–471.

Yang J-M, Tung C-H. 2006. Protein structure database search and evolutionary classification. *Nucleic Acids Res* **34**: 3646–3659.

Yedidi RS, Wendler P, Enenkel C. 2017. AAA-ATPases in protein degradation. *Front Mol Biosci* **4**: 42.

Zeytuni N, Strynadka NCJ. 2020. A hybrid secretion system facilitates bacterial sporulation: A structural perspective. *Microbiol Spectr* 9.

Zhang S, Mao Y. 2020. AAA+ ATPases in protein degradation: structures, functions and mechanisms. *Biomolecules* **10**: E629.